Understanding the nature and location of hydroxyl groups on hydrated titania nanoparticles

Understanding the Nature and Location of Hydroxyl Groups on Hydrated Titania Nanoparticles

Lorenzo Mino,[1,*] Ángel Morales-García,[2,*] Stefan T. Bromley,[2,3] Francesc Illas[2]

1) *Department of Chemistry and NIS Centre, University of Torino, via Giuria 7, 10125 Torino, Italy*

2) *Departament de Ciència de Materials i Química Física & Institut de Química Teòrica i Computacional (IQTCUB), Universitat de Barcelona, c/ Martí i Franquès 1-11, 08028 Barcelona, Spain*

3) *Institució Catalana de Recerca i Estudis Avançats (ICREA), Passeig Lluis Companys 23, 08010 Barcelona, Spain*

[*]Corresponding authors: lorenzo.mino@unito.it, angel.morales@ub.edu

Abstract

TiO_2 nanoparticles (NPs) are intensively studied and widely used due to their huge potential in numerous applications involving their interaction with ultraviolet light (e.g. photocatalysis, sunscreens). Typically, these NPs are in water-containing environments and thus tend to be hydrated. As such, there is a growing need to better understand the physicochemical properties of hydrated TiO_2 NPs in order to improve their performance in photochemical applications (e.g. photocatalytic water splitting) and to minimise their environmental impact (e.g. potential biotoxicity). To help address the need for reliable and detailed data on how nano-titania interacts with water, we present a systematic experimental and theoretical study of surface hydroxyl (OH) groups on photoactive anatase TiO_2 NPs. Employing well-defined experimentally synthesised NPs and detailed realistic NP models, we obtain the measured and computed infrared spectra of the surface hydroxyls, respectively. By comparing the experimental and theoretical spectra we are able to identify the type and location of different OH groups in these NP systems. Specifically, our study allows us to provide unprecedented and detailed information about the coverage-dependent distribution of hydroxyl groups on the surface of experimental titania NPs, the degree of their H-bonding interactions and their associated assigned vibrational modes. Our work promises to lead to new routes for developing new and safe nanotechnologies based on hydrated TiO_2 NPs.

† Electronic supplementary information (ESI) available: Tables with the list of OH vibrational modes. Fig. S1 correspond to the hydrated $(TiO_2)_{12}$ nanocluster. Finally, the atomic coordinated of all hydrated TiO_2 NPs are compiled in the *xyz* format. See DOI: .

1. Introduction

Titania (TiO_2) is a reducible oxide which, due to its role as a catalyst support and its many applications in photocatalysis, has been the subject of thousands of scientific studies and numerous reviews.[1-4] From a fundamental perspective, the atomic and electronic structure of the most common polymorphs of titania, namely rutile, anatase and brookite, have been studied by a wide range of experimental and theoretical methods.[5-7] For the bulk solids, these investigations generally agree on the electronic structure of the stoichiometric and reduced phases.[4,8-11] To control the catalytic and photocatalytic activity of titania, it is particularly important to understand the physics and chemistry of titania surfaces.[4,12-14] Single crystal samples with well-defined surfaces can be synthesized and under well controlled conditions[15,16] and, thereby, the low Miller index surfaces of rutile and anatase have been probed in detail by microscopy.[17] These systems are often used as simplified models for real titania catalysts in both experiment and theory. Through such studies, a reasonable consensus regarding the surface chemistry of extended titania surfaces has been achieved.[4] In spite of the huge effort in characterizing extended titania surfaces, real titania catalysts are made of nanoparticles (NPs).[18] Unlike clean extended surfaces, realistic titania NPs typically exhibit structurally complex surface features (e.g. edges, corners), and, depending on the environment, are partially covered absorbates (e.g. hydroxyl groups). In this work, we combine experiment and theory to provide unprecedented detailed insights into the surface chemistry of realistic hydroxylated titania NPs.

Although commercial titania NP photocatalysts such as P25 have been intensively studied with respect to better understanding their activity and composition,[19-21] a detailed atomic level description of their surface chemistry is still largely lacking. To reach a better understanding of these systems, experimental protocols have been developed to synthesize titania NPs with controlled shape and morphology.[22] NPs of the most photoactive anatase polymorph typically show a slightly truncated bipyramid shape formed by a majority of (101) facets and minority of (001) facets, as predicted by the Wulff construction.[23] Although the most stable (101) surface has attracted most attention,[24] recent studies have shown that it is possible to obtain anatase NPs with a large fraction of exposed reactive (001) facets.[25,26,27] Such results highlight the capacity of modern synthetic techniques to deliberately engineer NP morphologies.[28,29] From the modelling viewpoint, significant advances have been made to rationalize the morphologies of titania NPs by consideration of surface free energies.[17,30,31] Based on such considerations, realistic models of bare anatase NPs containing more than 1000 atoms have been studied by means of state-of-the-art density functional theory (DFT) based methods.[32-34] From such large scale electronic structure calculations it has been possible to determine the energy level alignment between anatase and rutile NPs and how this depends on size.[35] However, contrary to the situation for bulk titania and its extended clean surfaces, where theoretical

models are reliable representations of the experimental situation, the link between theoretical NP models and experimental NPs is more complicated. One reason for the gap between theory and experiment is that titania NPs are highly sensitive to hydroxylation, which is unavoidable in real world environments. Given that one of the main applications of titania NPs is for the photocatalytic splitting of water, such NPs are unavoidably in contact with water. Hydroxylation can significantly affect the (photo)catalytic properties of titania NPs,[36-39] and is also likely linked to the degree of bio-toxicity of these NP species.[40] Indeed, the density and location of surface hydroxyl groups is thought to play a fundamental role in biomolecule adsorption at titania surfaces.[41]

Up to now, most theoretical models of titania NPs have been mainly focused on anhydrous systems. Several computational investigations have been performed on extended rutile (110), and anatase (101) and (001) surfaces to understand water adsorption structure and the equilibrium between water adsorbed in molecular and dissociative form.[42-50] However, the use of extended surface models does not allow for the realistic analysis of the properties of finite corner and edge regions which are likely to have particular reactivities. A recent theoretical study reported that water molecules bind strongly at the surface of anatase NPs with an exothermic hydration energy (E_{hyd}). The largest E_{hyd} values were found for uncoordinated Ti atoms at NP corners and progressively decreased for edges and then facet surface sites.[51] More recently, the properties of very small hydrated titania NPs (*i.e.*, nanoclusters) were analysed using *ab initio* atomistic thermodynamics.[52] Titania nanoclusters have high surface to bulk ratios and possess many atoms with lower than bulk coordination and were predicted to be significantly hydroxylated, even under ambient conditions. These preliminary theoretical studies strongly suggest that nano-sized titania species are likely to be highly hydroxylated, but, without comparison with detailed characterizations from experiment, these predictions cannot be confirmed. Clearly, for a more detailed and deeper understanding of the dissociation of water to form hydroxyls on titania NPs, the use of realistic NP models is essential.

To close the gap between experiment and theoretical models, we report a systematic study of hydrated anatase NPs where, the coverage of hydroxyl groups was controlled in both the experiments and the theoretical models. On the experimental side, we synthesized shape-controlled bipyramidal NPs, with dominant (101) facets, and compared them with widely employed commercial titania NPs by precisely tuning the hydroxylation degree. In the theoretical modelling we constructed, realistic anatase faceted NPs covered by a different number of hydroxyl groups occupying well defined sites. Careful comparison of the measured and computed infrared (IR) vibrational spectra allowed us to directly determine the types and location of the hydroxyl groups on these anatase titania NPs. Our work thus provides unprecedented and detailed insights into the interaction of this hugely important photocatalytic nanomaterial with aqueous environments.

2. Methods

2.1 Materials and characterisation techniques

TiO_2 nano-anatase NPs (BET specific surface area = 140 $m^2 g^{-1}$) were purchased from Sigma-Aldrich. TiO_2 P25 NPs (specific BET surface area = 60 $m^2 g^{-1}$, ~85 % anatase and ~15 % rutile) were purchased from Evonik. Shape-controlled bipyramidal TiO_2 anatase NPs (specific BET surface area = 40 $m^2 g^{-1}$), hereafter named TiO_2 bipy, were obtained by forced hydrolysis of a 40 mM aqueous solution of triethanolamine complex at pH 10, carried out by hydrothermal treatment at 453 K for 90 hours in autoclave, as described in detail in previous publications.[53,54] High resolution transmission electron microscopy (HR-TEM) images of the NPs (powder grains "dry" dispersed on lacey carbon Cu grids) were acquired using a JEOL 3010-UHR microscope operated at 300 kV. For Fourier-transform IR (FTIR) spectroscopy, the samples were pressed in self-supporting pellets ("optical density" of ca. 10 $mg \cdot cm^{-2}$) and placed in quartz cells equipped with KBr windows designed to carry out spectroscopic measurements in controlled atmosphere. The cells were connected to a conventional vacuum line (residual pressure: 1×10^{-5} mbar) allowing all thermal treatments and adsorption-desorption experiments to be carried out *in situ*. After each thermal treatment, the samples were oxidized with O_2 at 15 mbar to obtain stoichiometric TiO_2. The thermal treatments performed on the NPs do not induce phase transitions or any significant decrease in the specific BET surface area, as thoroughly checked in previous studies.[20,21,55] A Bruker IFS 66 spectrometer, equipped with an MCT detector, was employed for the FTIR spectra collection, averaging 128 scans at 2 cm^{-1} resolution.

2.2 Computational methodology

Realistic anhydrous $(TiO_2)_{35}$ and $(TiO_2)_{84}$ NP models composed of 105 and 252 atoms, respectively were first made employing the Wulff construction to cut the bulk anatase crystal following a top-down approach.[32] Both NPs are display octahedral symmetry and exhibit the most stable (101) surface on all facets (see Fig. 1). These NPs were selected based on the increasing structural stability of such faceted NP morphologies with increasing size, in comparison with other NP shapes (e.g. spherical).[34] Previous work provides compelling evidence that the largest $(TiO_2)_{84}$ NP is in the scalable size regime in which properties linearly vary with size towards bulklike limit values.[32,56] Water molecules were added to each NP in a dissociative way following the progressively decreasing order of reactivity of the surface regions (*i.e.* apical vertices, equatorial corners, edges and facets). Here, we assume that the water interaction is dissociative and heterolytic thus involving H^+ and OH^- groups, whereby the proton interacts with under-coordinated O atoms and the hydroxyl bonds to under-coordinated Ti atoms located on the NP surface. Hydrated TiO_2 NPs were thereby constructed with ~38% and ~88% water with respect to the total number of water molecules needed to totally cover the corresponding

anhydrous NP surface Specifically, NPs with 38% water coverage correspond to $(TiO_2)_{35}(H_2O)_{13}$ and $(TiO_2)_{84}(H_2O)_{24}$ stoichiometries, and those with 88% coverage correspond to, $(TiO_2)_{35}(H_2O)_{30}$, and $(TiO_2)_{84}(H_2O)_{55}$ stoichiometries.

The atomic structure of all NPs was relaxed using Density Functional Theory (DFT) based calculations explicitly including all electrons as implemented in the Fritz Haber Institute *ab initio* molecular simulations (FHI-aims) package,[57] and employing the Perdew-Burke-Ernzerhof (PBE) exchange-correlation density functional.[58] The electron density was described through a light grid and tier-1 numerical atom-centered orbital (NAO) basis set, which ensures an accuracy comparable to a TZVP Gaussian type orbital basis set.[32] The convergence threshold for atomic forces during the final relaxation of the structure was set to 10^{-4} eV $Å^{-1}$ both for bare and hydrated TiO_2 NPs. Relativistic effects were also included through the zero-order regular approximation (ZORA).[59]

The harmonic vibrational frequencies and intensities were computed by diagonalizing the mass-weighted Hessian matrix, obtained using a finite difference approach. To calculate the vibrational frequencies, only the surface OH groups were considered, after confirming that they were not significantly coupled to other bulk-like vibrational modes. We note that this approximation led to differences of < 0.5 cm^{-1} with respect to full frequency calculations involving also all the atoms of the NP. This computational strategy allowed us to reduce the highly demanding computational cost required to study these large systems. We determined a suitable factor (f = 0.9806) to scale the theoretically computed frequencies to best match experimental values. This was done by comparing the values of experimental and computed frequencies of water in gas phase, considering an average between ν_{asym} and ν_{sym} modes, according to the following formula:

$$f = \frac{1}{2}\left(\frac{\nu_{asym,exp}}{\nu_{asym,comp}} + \frac{\nu_{sym,exp}}{\nu_{sym,comp}}\right)$$

In addition, a small hydrated $(TiO_2)_{12}(H_2O)_5$ nanocluster (NC) taken from ref. 52 (see Fig S1 in ESI) was considered to analyse the effect of the choice of the basis set and computational parameters in the calculation of the frequencies. Only very small differences (< 5 cm^{-1}) were observed in all test calculations, thus confirming that the tier 1 light basis set was suitable to perform the frequency analysis for our larger TiO_2 NPs. The $(TiO_2)_{12}(H_2O)_5$ NC also possesses hydroxylated tetrahedrally coordinated Ti atoms that are not found in our bulk-like faceted TiO_2 NPs models. The relatively high frequencies of these specific hydroxyls on the NC were also found to be useful for rationalising one of the experimental IR peaks, as discussed below

3. Results and discussion

In the following, we start with a detailed discussion of the results of the FTIR experiments in controlled atmosphere. In the second subsection, the water dissociation energetics and the simulated

IR spectra based on DFT calculations are analysed. Finally, we compare our experimental findings with our theoretical predictions.

3.1 FTIR spectroscopy

Starting with the experiments, three different TiO_2 NPs were investigated in the present study. Two of them, Aldrich nano-anatase and Evonik P25 TiO_2 NPs, were selected since they are widely employed in practical applications and because they do not show the presence of species trapped in internal cavities or strongly bound surface chemical impurities, which are often present in NPs prepared from wet chemistry synthesis.[60] The third one, a shaped-controlled TiO_2 bipy sample, was synthetized by some of us as described in previous studies.[53,54] Note that this latter sample, showing a truncated bipyramid shape (see TEM image in Fig. 2) dominated by {101} facets (> 90%),[53] is the most straightforwardly comparable with the computational models (see Fig. 1). However, the Aldrich nano-anatase and Evonik P25 TiO_2 NPs, although showing a more heterogeneous distribution of the NPs size and shape, as visible in the TEM images reported in the right part of Fig. 2, also mainly expose {101} facets. This feature is also clearly highlighted by previous high-resolution TEM investigations combined with IR studies employing CO as probe molecule.[20,21,53] The chemical and phase purity, the high specific surface area and the predominance of {101} facets make Aldrich nano-anatase a very suitable system to be compared with our computational predictions as shown later.

Since our study is focused on hydroxyl groups, before acquiring the IR spectra, we outgassed the samples at high temperature (see Methods section for further details) to selectively remove molecular water and all other adsorbed contaminants. The FTIR spectra of all TiO_2 NPs after the thermal treatments are shown in Fig. 2. Interestingly, all samples show four main common IR bands, associated to the hydroxyl ν(OH) stretching mode, centred at 3737-3735 (as a shoulder for the P25 sample), 3718-3715, 3696-3689 (this wide range could be also due to the presence of a small contribution of OH groups in the rutile fraction of P25)[61] and 3671 cm^{-1}. A low frequency component at 3643-3642 cm^{-1} is also present in the nano-anatase and P25 spectra. The experimental assignments of these signals reported in the literature are often based on the interpretation proposed in pioneering studies dating back to the 1970s that indicated that terminal hydroxyls vibrate at higher frequencies than bridging hydroxyl.[62,63] Therefore, bands above 3700 cm^{-1} are generally ascribed to terminal OHs, while those at lower frequencies are associated to bridging OHs.[64,65] However, more recent DFT studies[61,66-69] employing periodic models have provided new insights and some of them questioned the previous assignments, showing that the frequencies of terminal OHs could be in some cases lower than those of bridging OHs.[61,66,] We note that, although extended periodic surface models can describe the facets found in TiO_2 NPs, important adsorption sites like edges, corners and apical sites are not represented at all. In contrast, the intrinsically finite and morphologically realistic NP models include

all adsorption sites. The comparison of our experimental data with the DFT results obtained by using realistic NPs models (Fig. 1) is expected to contribute to clarify the controversial issue of where water preferentially adsorbs on these nano-TiO_2 species, as we discuss below.

3.2 DFT calculations

Our $(TiO_2)_{35}$ and $(TiO_2)_{84}$ NP models all show the same octahedral morphology and, hence, expose analogous surface zones (*i.e.* apical vertices, corners in the equatorial region, edges connecting apical and corner regions, and (101) surface facets). To assess NP reactivity with respect to dissociative water addition, we calculated the incremental hydration energy (ΔE_{hyd}):

$$\Delta E_{hyd} = E_{hyd}[(TiO_2)_n(H_2O)_m] - E_{hyd}[(TiO_2)_n(H_2O)_{m+1}]$$

and

$$E_{hyd} = E[(TiO_2)_n(H_2O)_m] - E[(TiO_2)_n] - m\,E_{hyd}[(H_2O)]$$

where m is the number of progressively added water molecules and n the number of TiO_2 units in the NP model (n = 35 or 84 in our case).

It is reasonable to assume that ΔE_{hyd} will be largest for low water coverage where the first water molecules can bind to the most reactive sites available. Conversely, when the water coverage starts to reach its upper saturating limit only the least reactive sites remain and ΔE_{hyd} is expected to be lowest. For both $(TiO_2)_{35}$ and $(TiO_2)_{84}$ based NP models similar tendencies are found for the evolution of ΔE_{hyd} with respect to the hydroxylation degree (see Fig. 3). For the initial dissociative adsorption of water on apical vertices we find ΔE_{hyd} to be highest with an associated energy gain of between 1.5 and 2.0 eV. Progressive hydroxylation of the equatorial corner sites leads to a slightly smaller energy gain of between 1.0-1.5 eV. The following hydroxylation of edge sites corresponds to average ΔE_{hyd} values around 0.5 eV. We note that few facet sites are also hydrated in case of the largest $(TiO_2)_{84}$ NP, with associated ΔE_{hyd} values being slightly above 0.5 eV. These results suggest that the magnitude of ΔE_{hyd} can be a used as an approximate descriptor of the location of any particular hydroxyl. As ΔE_{hyd} tends to converge to its minimum value with increasing coverage, we can also use the magnitude of ΔE_{hyd} to indicate the degree of hydration. This convergence is most clearly observed with the larger $(TiO_2)_{84}$ based NP model (see Fig. 3). In summary, our analysis confirms that the hydroxylation of vertices is the most exothermic followed by corners, and edges in agreement with previous studies.[51]

In Fig. 4a we summarise the scaled OH frequencies of our $(TiO_2)_{35}(H_2O)_{13}$ NP model, which possesses 26 OH groups. We observe that the majority of the scaled OH frequencies are grouped in the 3710-3650 cm^{-1} spectral range, which is in good agreement with the experimental IR vibrational spectra measured after outgassing the samples at 773 K (see Fig. 2). However, we also find a few

vibrations around 3500 and 3300 cm^{-1}, corresponding to hydroxyls interacting with neighbouring hydroxyls via strong hydrogen bonds. Increasing the number of OH groups from 26 to 60 to reach 88% coverage in the $(TiO_2)_{35}(H_2O)_{30}$ NP model (see Fig. 4b), the possibilities for inter-hydroxyl hydrogen bonding also increase with a concomitant increase in the number of vibrational peaks in the frequency range between 3600-3100 cm^{-1}. As the $(TiO_2)_{35}(H_2O)_{30}$ model is already close to full coverage, it is limited in the extent to which it can capture a broad range of different OH sites/interactions potentially present in the experimental NPs.

To overcome the limitations of the $(TiO_2)_{35}$ NP model, we consider the considerably larger $(TiO_2)_{84}$ model and consider coverages close to 38% and 88%, corresponding to the dissociative addition of 24 and 55 water molecules respectively. The simulated IR spectrum of the $(TiO_2)_{84}(H_2O)_{24}$ NP exhibits peaks of free and weakly hydrogen bonded OH groups, but does not provide a basis for the assignment of the experimentally observed features below 3400 cm^{-1}. In stark contrast, the higher coverage $(TiO_2)_{84}(H_2O)_{55}$ NP model shows an almost continuous series of vibrational peaks in the range 3000-3600 cm^{-1} (see Fig. 4d). We find that this larger NP with high water coverage is the most satisfactory model to interpret the present experimental results as we discuss in detail below. We note that the full list of computed IR vibrations depicted in Fig. 4 are listed in the ESI.

3.3 Comparison between experimental and computational results

To facilitate the comparison between experimental and computational results, Fig. 5 reports the simulated IR spectra for the largest NP model, $(TiO_2)_{84}(H_2O)_{55}$, and two experimental spectra of TiO_2 nano-anatase, outgassed at different temperatures. The sample treated in vacuum at 773 K (red spectrum in Fig. 5), as already mentioned in the discussion of Fig. 1, has only IR signals in the 3750-3600 cm^{-1} range, ascribed to free OH groups. On the contrary, the NPs outgassed at 673 K (black spectrum in Fig. 5) show also a broad absorption band extending down to 3000 cm^{-1}, due to hydrogen bonded hydroxyls. The absence of the bending mode at 1620 cm^{-1} excludes the presence of undissociated water molecules in the latter sample. We note that the intensity of the OH vibrations above 3700 cm^{-1} is not significantly affected by the increase of the outgassing temperature from 673 to 773 K, suggesting that these IR signals are related to strongly bound OH groups. These hydroxyls are likely located on vertices and corners, which show the highest ΔE_{hyd} (see Section 3.2). This hypothesis is further confirmed by the analysis of the IR vibrations in the $(TiO_2)_{84}(H_2O)_{55}$ NP shown in Fig. 5. Indeed, the computed frequencies above 3700 cm^{-1} correspond to isolated OH groups localized in the apical region of the NPs. In addition, two more modes in this range, correspond to OH groups located in the edge regions close to the apical vertices vibrating in a cooperative and symmetrical manner. The higher frequency component ~3735 cm^{-1} (marked by a blue star in the experimental spectrum in Fig. 5) could not be identified in the vibrational spectrum of the

$(TiO_2)_{84}(H_2O)_{55}$ NP. Interestingly, however, this mode is well matched by a mode in the computed vibrational spectrum of the small hydrated $(TiO_2)_{12}(H_2O)_5$ nanocluster model (Fig. S1 in the ESI). We find that this mode corresponds to a particular type of isolated OH group linked to a tetrahedrally coordinated Ti atom. The larger NP models are based on clean bulk cuts of anatase, and do not exhibit such sites. This implies that the surfaces of the anatase NPs in experiments possess some coordination-lowering surface defects which are not captured by our ideal bulk-cut NPs models. The region between 3700 and 3600 cm^{-1} correspond to free OH groups located on the edges of the NPs. The weakly and strongly H-bonded OH groups located simultaneously in the equatorial and edge regions are responsible for modes in the 3600-3300 and 3300-3000 cm^{-1} ranges (see assignment in the upper left of Fig. 5). To rationalize these computational finding with respect to the experiment spectra, we assume that the weakly and strongly H-bonded OH groups confirmed to be present by the FTIR at 673 K can diffuse to form water molecules that desorb from the NP at 773 K, leading to the significant decrease of the intensity broad band from 3500-3000 cm^{-1}. At this higher temperature, isolated OH groups in apical and edge regions remain anchored to the NP and give rise to the remaining experimental signal in this region, in broad agreement with our computational results (see comparison of experimental and computational spectra to the left in Fig. 5). Our interpretation provides an overview of how and where water dissociatively interacts with realistic TiO_2 NPs,which promotes the covering of the NP surface by OH groups. However, further analysis is needed to better investigate the molecular mechanism of this process. In summary, the present joint computational and experimental study provides new detailed insights into the nature of OH species on hydrated titania NPs. Specifically, through a detailed comparison of experimental FTIR spectra and accurately computed IR spectra, we are able to identify the likely location and degree of H-bonding interactions of OH groups on realistic synthesised anatase NPs.

4. Conclusions

We have carried out a combined theoretical and experimental study to investigate the location, chemical environment and vibrational modes of hydroxyl (OH) groups bound to the surface of titania NPs. We compared experimental IR spectra of three different anatase-based TiO_2 NP samples (namely nano-anatase, P25, and shaped controlled bypiramidal NPs) with the simulated IR spectra of hydrated bypiramidal anatase NP models possessing ~38 and ~88% water coverages. We thus show that a $(TiO_2)_{84}(H_2O)_{55}$ NP model with a high hydroxyl coverage allows us to rationalize the frequencies observed in the experimental FTIR spectra and to relate these modes to types of OH species at localized regions of the NP. We also find that the broad IR signals between 3600 and 3000 cm^{-1} can be ascribed to weakly and strongly H-bonded OH groups, which tend to form water molecules that desorb upon increasing the outgassing temperature to 773 K. The resulting outgassed

NPs show a well-defined FTIR spectrum in the 3750-3600 cm^{-1} spectral region, corresponding to free OH groups. The components above 3700 cm^{-1} are related to hydroxyl groups located in the apical regions of the bypiramidal $(TiO_2)_{84}(H_2O)_{55}$ NP and to Ti-OH sites in which Ti is tetrahedrally coordinated. This assignment agrees with the fact that such regions have relatively higher reactivity and, thus, water dissociation is more favourable (corresponding to their higher ΔE_{hyd} values), generating strongly bound OH groups. Finally, the signals between 3700 and 3600 cm^{-1} are mainly due to isolated hydroxyls located on edges.

Overall, our collaborative study demonstrates how experiment and theory can provide unprecedented quantitative insights in the detailed surface chemistry of complex inorganic nanosystems. Specifically, we provide otherwise unobtainable information about the distribution of the surface hydroxyl groups on the surface of titania NPs, the degree of their H-bonding interactions and their vibrational modes. There is a burgeoning need to better understand the physicochemical properties of widely used hydrated nano-TiO_2 NPs with respect to improving their performance in photochemical applications (e.g. photocatalytic water splitting), safe usage in products (e.g. sunscreens) and reducing their possible environmental impact (e.g. potential biotoxicity of titania NPs). Our study could pave the way for new routes for improved control and development of new and safe TiO_2 NP-based nanotechnologies.

Conflicts of interest

There are no conflicts to declare

Acknowledgements

L. M. gratefully acknowledges the Italian Ministry of Education, University and Research (MIUR) for supporting his stay at the Universitat de Barcelona through the “Leonardo da Vinci 2019” action. A. M.-G. thanks to *Ministerio de Ciencia e Investigación* for the *Juan de la Cierva* postdoctoral grant (IJCI-2017-31979) and F. I. acknowledges additional support from the 2015 ICREA Academia Award for Excellence in University Research. This research was supported by the Spanish *Ministerio de Ciencia e Innovación* RTI2018-095460-B-I00 and *María de Maeztu* program through grant MDM-2017-0767 and, in part, by *Generalitat de Catalunya* (grant 2017SGR13) and COST Action CA18234. Computational time at the MareNostrum supercomputer has been provided by the Barcelona Supercomputing Centre (BSC) through the grant of the Partnership for Advanced Computing in Europe (PRACE) under the EXCIPHOCAT project (2016163940).

Fig. 1 Anhydrous bipyramidal $(TiO_2)_{35}$ and $(TiO_2)_{84}$ NPs and their hydrated counterparts $(TiO_2)_{35}(H_2O)_{13}$, $(TiO_2)_{35}(H_2O)_{30}$, $(TiO_2)_{84}(H_2O)_{24}$, and $(TiO_2)_{84}(H_2O)_{55}$ employed in this study. Horizontal and vertical arrows indicate the NP hydration and size, respectively. Blue, red and white spheres correspond to Ti, O, and H atoms, respectively.

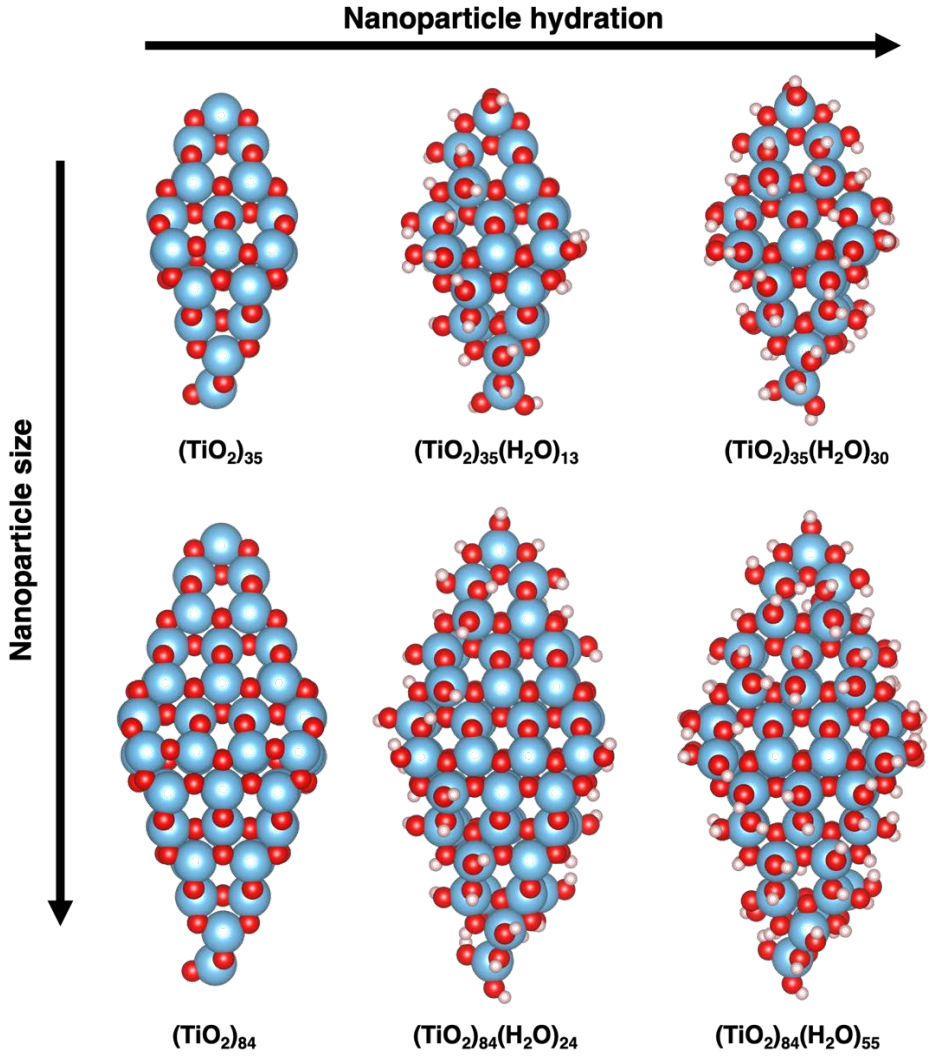

Fig. 2 Left: FTIR spectra of the TiO_2 nano-anatase (blue), TiO_2 bipy (black) and TiO_2 P25 NPs (red) after outgassing at 773 K. Right: TEM images of the respective samples.

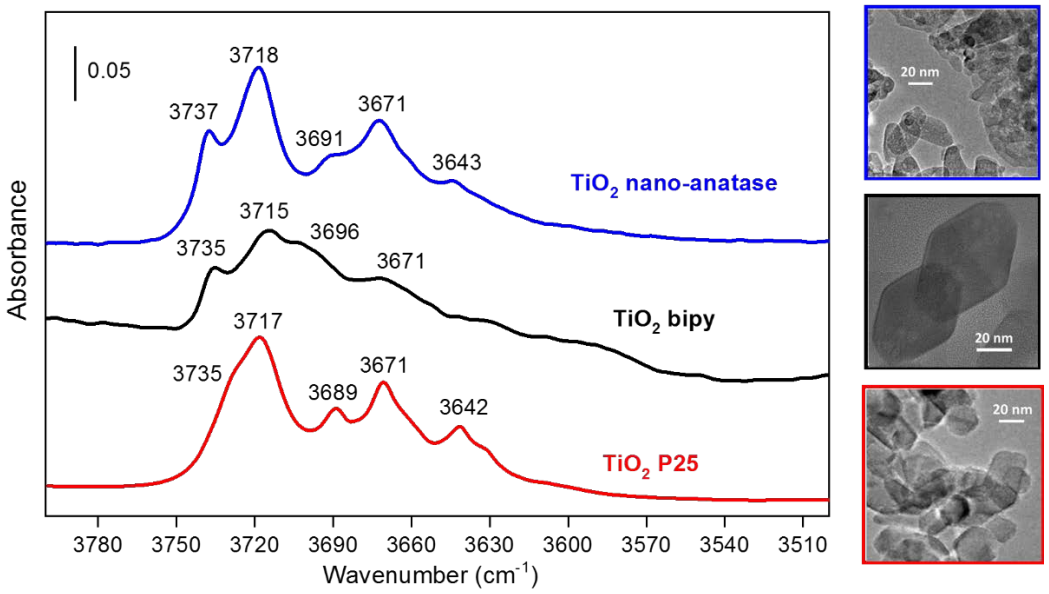

Fig. 3 Evolution of ΔE_{hyd} with the number of water molecules (m) for increasingly hydrated $(TiO_2)_{35}(H_2O)_m$ and $(TiO_2)_{84}(H_2O)_m$ NPs. Coverages of different types of NP surface regions for different ranges of m are separated by vertical dashed lines.

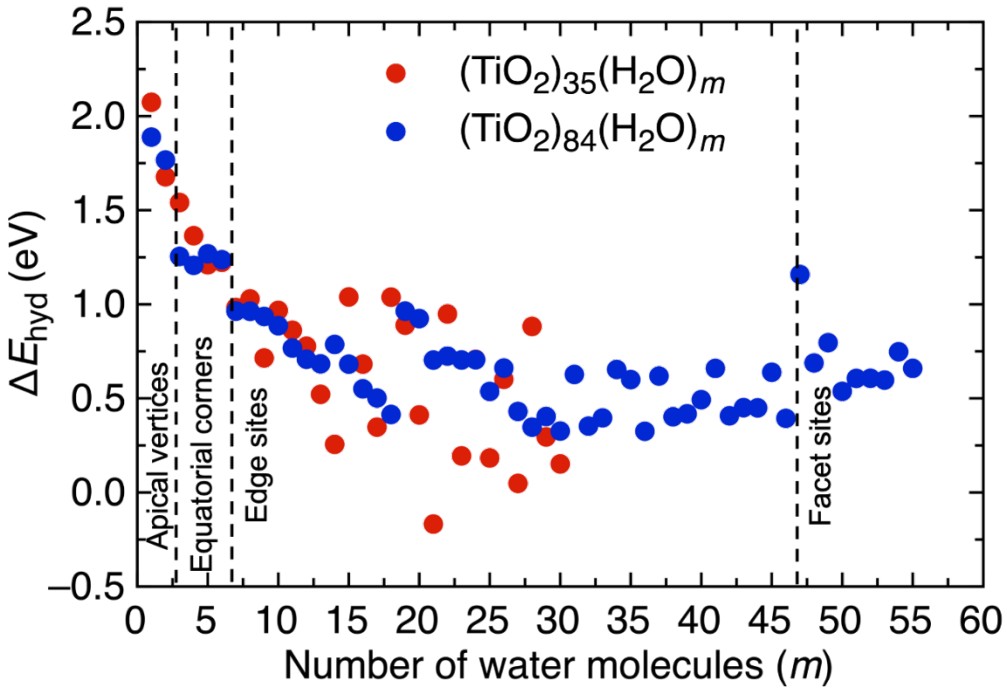

Fig. 4 Simulated IR spectra of (a) $(TiO_2)_{35}(H_2O)_{13}$, (b) $(TiO_2)_{35}(H_2O)_{30}$, (c) $(TiO_2)_{84}(H_2O)_{24}$, and (d) $(TiO_2)_{84}(H_2O)_{55}$ NPs. The red line represents the resulting IR spectra, whereas the vertical black lines indicate the computed harmonic frequencies.

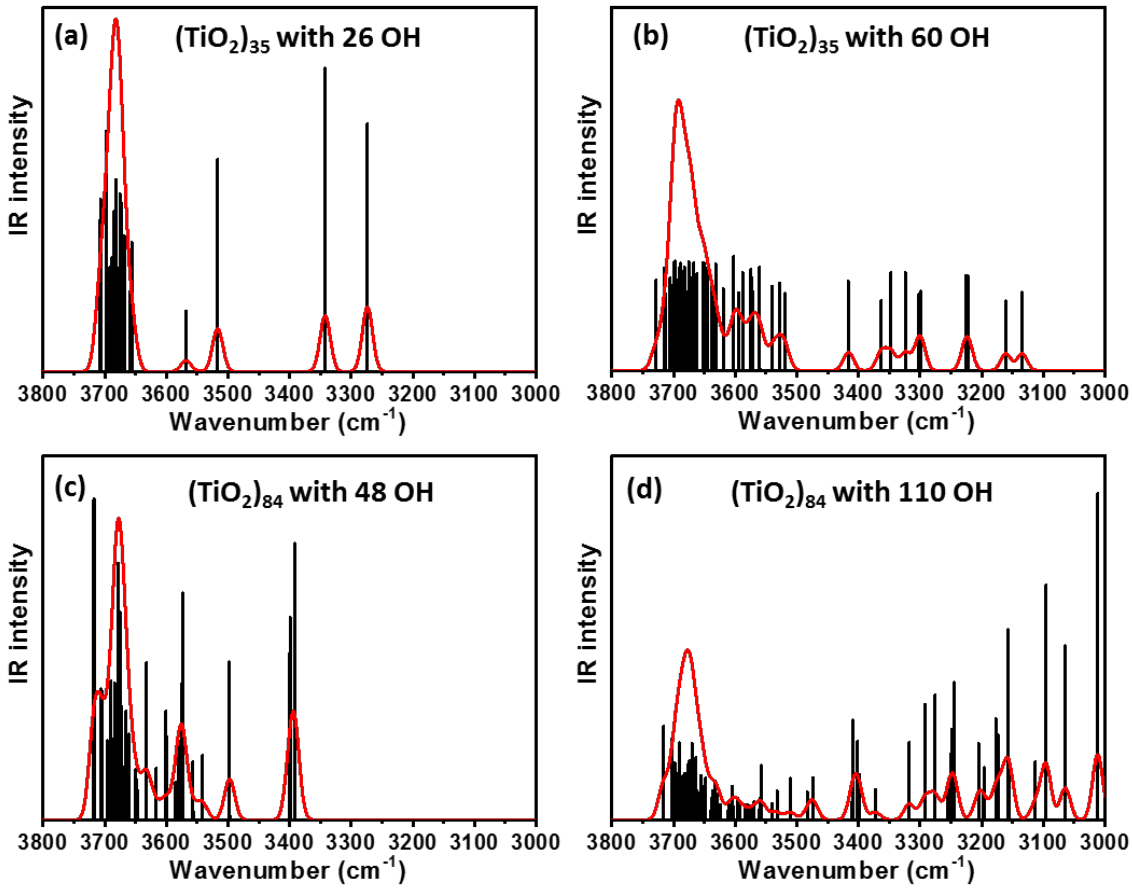

Fig. 5 Calculated IR frequencies (top left panel) obtained from the $(TiO_2)_{84}(H_2O)_{55}$ NP model (right – note that two orientations of the NP are shown) compared to the FTIR spectra of the TiO_2 nano-anatase NPs (bottom left panel) after outgassing at 773 K (red curve) or 673 K (black curve). Vibration modes are distinguished by a colour scale, where the highest frequencies are found towards the purple end of the scale and and the lowest frequencies are identified by colours towards the red end of the scale. The same colour scale is used to correlate the OH groups ss in the $(TiO_2)_{84}(H_2O)_{55}$ NP model with their respective frequencies. Note that the Ti and O atoms that form the core of the NP are depicted with light and dark grey colours, respectively. The blue star on the FTIR spectra of the TiO_2 nano-anatase NPs indicates the frequency of a single tetrahedrally coordinated OH (see IR spectrum of the $(TiO_2)_{12}$ NP in the SI).

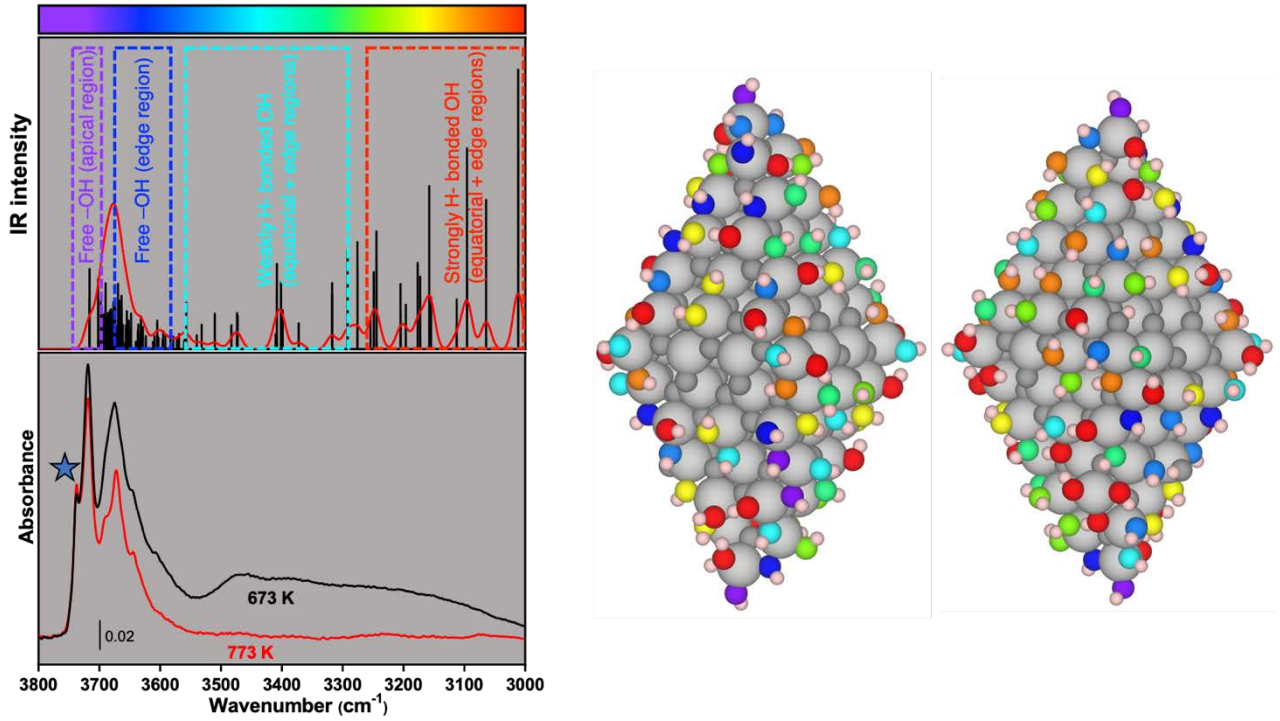

References

(1) X. Chen and S. S. Mao, *Chem. Rev.*, 2007, **7**, 2891-2959.

(2) X. Chen and A. Selloni, *Chem. Rev.*, 2014, **144**, 9281-9282.

(3) G. Liu, H. G. Yang, J. Pan, Y. Q. Yang, G. Q. Lu and H.-M. Cheng, *Chem. Rev.*, 2014, **144**, 9559-9612.

(4) R. Rousseau, V. A. Glezakou, A. Selloni, *Nat. Rev. Mater.*, 2020, **5**, 460–475.

(5) Y. Ma, X. Wang, Y. Jia, X. Chen, H. Han and C. Li, *Chem. Rev.*, 2014, **114**, 9987-10043.

(6) A. Di Paola, M. Bellardita and L. Palmisano, *Catalysts*, 2013, **3**, 36-73.

(7) M. Monai, T. Montini and P. Fornasiero, *Catalysts*, 2017, **7**, 304 (1-19).

(8) M. K. Nowotny, T. Bak and J. Nowotny, *J. Phys. Chem. B*, 2006, **110**, 16270-16282.

(9) S. Tosoni, O. Lamiel-García, D. Fernández-Hevia, J. M. Doña and F. Illas, *J. Phys. Chem. C*, 2012, **116**, 12738-12746.

(10) X. Pan, M.-Q. Yang, X. Fu, N. Zhang and Y.-J. Xu, *Nanoscale*, 2013, **5**, 3601-3614.

(11) K. C. Ko, O. Lamiel-García, J. Y. Lee and F. Illas, *Phys. Chem. Chem. Phys.*, 2016, **18**, 12357-12367.

(12) U. Diebold, *Surf. Sci. Rep.*, 2003, **48**, 53-229.

(13) A. Fujishima, X. Zhang and D. A. Tryk, *Surf. Sci. Rep.*, 2008, **63**, 515-582.

(14) H. Xu, S. Ouyang, L. Liu, P. Reunchan, N. Umewaza and J. Ye, *J. Mater. Chem. A*, 2014, **2**, 12642-12661.

(15) T. Butburee, P. Kotchasarn, P. Hirunsit, Z. Sun, Q. Tang, P. Khemthong, W. Sangkhun, W. Thongsuwan, P. Kumnorkaew, H. Wang and K. Faungnawakij, *J. Mater. Chem. A*, 2019, **7**, 8156-8166.

(16) S. Yang, B. X. Yang, L. Wu, Y. H. Li, P. Liu, H. Zhao, Y. Y. Yu, X. Q. Gong and H. G. Yang, *Nat. Commun.*, 2014, **5**, 5355.

(17) H. Zhang and J. F. Banfield, *Chem. Rev.*, 2014, **114**, 9613-9644.

(18) Y.-K. Peng, Y. Hu, H.-L. Chou, Y. Fu, I. F. Teixeira, L. Zhang, H. He and S. C. E. Tsang, *Nat. Commun.*, 2017, **8**, 675.

(19) D. C. Hurum, A. G. Agrios, K. A. Gray, T. Rajh and M. C. Thurnauer, *J. Phys. Chem. B*, 2003, **107**, 4545-4549.

(20) L. Mino, G. Spoto, S. Bordiga and A. Zecchina, *J. Phys. Chem. C*, 2012, **116**, 17008-17018.

(21) L. Mino, G. Spoto, S. Bordiga and A. Zecchina, *J. Phys. Chem. C*, 2013, **117**, 11186-11196.

(22) G. Liu, J. C. Yu, G. Q. Lu and H.-M. Cheng, *Chem. Commun.*, 2011, **47**, 6763-6783.

(23) L. Mino, A. M. Ferrari, V. Lacivita, G. Spoto, S. Bordiga and A. Zecchina, *J. Phys. Chem. C*, 2011, **115**, 7694-7700.

(24) A. V. Vorontsov, H. Valdés, P. G. Smirniotis and Y. Paz, *Surfaces*, 2020, **3**, 72-92.

(25) S. Liu, J. Yu and M. Jaroniec, *Chem. Mater.*, 2011, **23**, 4085-4093.

(26) H. G. Yang, C. H. Sun, S. Z. Qiao, J. Zou, G. Liu, S. C. Smith, H. M. Cheng and G. Q. Lu, *Nature*, 2008, **453**, 638-641.

(27) Y. X. Zhao, Y. F. Zhao, R. Shi, B. Wang, G. I. N. Waterhouse, L. Z. Wu, C. H. Tung and T. R. Zhang, *Adv. Mater.*, 2019, **31**, 1806482.

(28) J. Pan, G. Liu, G. Q. Lu and H.-M. Cheng, *Angew. Chem. Int. Ed.*, 2011, **50**, 2133-2137.

(29) Y. Alivov and Z. Y. Fan, *J. Phys. Chem. C*, 2009, **113**, 12954-12957.

(30) H. Zhang and J. Banfield, *J. Mater. Chem.*, 1998, **8**, 2073-2076.

(31) A. S. Barnard and L. A. Curtiss, *Nano Lett.*, 2005, **5**, 1261-1266.

(32) O. Lamiel-García, K. C. Ko, J. Y. Lee, S. T. Bromley and F. Illas, *J. Chem. Theory Comput.*, 2017, **13**, 1785-1793.

(33) Á. Morales-García, R. Valero and F. Illas, *Phys. Chem. Chem. Phys.*, 2018, **20**, 18907-18911.

(34) Á. Morales-García, A. M. Escatllar, F. Illas and S. T. Bromley, *Nanoscale*, 2019, **11**, 9032-9041.

(35) K. C. Ko, S. T. Bromley, J. Y. Lee and F. Illas, *J. Phys. Chem. Lett.*, 2017, **8**, 5593-5598.

(36) X.-Q. Gong and A. Selloni, *J. Phys. Chem. B*, 2005, **109**, 19560-19562.

(37) M. L. Weichman, S. Debnath, J. T. Kelly, S. Gewinner, W. Schöllkpf, D. M. Neumark and K. R. Asmis, *Top Catal.*, 2018, **61**, 92-105.

(38) L. Mino, C. Negri, A. Zecchina and G. Spoto, *Z. Phys. Chem.*, 2016, **230**, 1441-1451.

(39) L. Mino, A. Zecchina, G. Martra, A. M. Rossi and G. Spoto, *Appl. Catal. B-Environ.*, 2016, **196**, 135-141.

(38) Y. Tanga, R. Caia, D. Caob, X. Konga, Y. Luc, *Toxicology*, 2018, **406-407**, 1–8.

(41) M. J. Limo, A. Sola-Rabada, E. Boix, V. Thota, Z. C. Westcott, V. Puddu and C. C. Perry, *Chem. Rev.*, 2018, **118**, 11118-11193.

(42) Z. T. Wang, Y. G. Wang, R. T. Mu, Y. Yoon, A. Dahal, G. K. Schenter, V. A. Glezakou, R. Rousseau, I. Lyubinetsky and Z. Dohnalek, *Proc. Natl. Acad. Sci. U. S. A.*, 2017, **114**, 1801-1805.

(43) J. Matthiesen, J. Ø. Hansen, S. Wendt, E. Lira, R. Schaub, E. Lægsgaard, F. Besenbacher and B. Hammer, *Phys. Rev. Lett.*, 2009, **102**, 226101.

(44) T. Zheng, C. Wu, M. Chen, Y. Zhang and P. T. Cummings, *J. Chem. Phys.*, 2016, **145**, 044702.

(45) Y. He, A. Tilocca, O. Dulub, A. Selloni and U. Diebold, *Nat. Mater.*, 2009, **8**, 585-589.

(46) L. E. Walle, A. Bong, E. M. J. Johansson, S. Plogmaker, H. Rensmo, P. Uvdal and A. Sandell, *J. Phys. Chem. C*, 2011, **115**, 9545-9550.

(47) R. Martínez-Casado, G. Mallia, N. M. Harrison and R. Pérez, *J. Phys. Chem. C*, 2018, **122**, 20736-20744.

(48) G. Fisicaro, S. Filice, S. Scalese, G. Compagnini, R. Reitano, L. Genovese, S. Goedcker, I. Deretzis and A. La Manga, *J. Phys. Chem. C*, 2020, **124**, 2406-2419.

(49) I. M. Nadeem, J. P. W. Treacy, S. Selcuk, X. Torrelles, H. Hussain, A. Wilson, D. C. Grinter, G. Cabailh, O. Bikondoa, C. Nicklin, A. Selloni, J. Zegenhagen, R. Lindsay and G. Thornton, *J. Phys. Chem. Lett.*, 2018, **9**, 3131-3136.

(50) X. Lang, Y. Liang, J. Zhang, L. Li, L. Cao and H. Zhang, *Phys. Chem. Chem. Phys.*, 2020, **22**, 1371-1380.

(51) D. R. Hummer, J. D. Kubicki, P. R. C. Kent and P. J. Heaney, *J. Phys. Chem. C*, 2013, **117**, 26084-26090.

(52) A. Cuko, A. M. Escatllar, M. Calatayud and S. T. Bromley, *Nanoscale*, 2018, **10**, 21518-21532.

(53) L. Mino, F. Pellegrino, S. Rades, J. Radnik, V. D. Hodoroaba, G. Spoto, V. Maurino and G. Martra, *ACS Appl. Nano Mater.*, 2018, **1**, 5355-5365.

(54) F. Pellegrino, F. Sordello, L. Mino, C. Minero, V. D. Hodoroaba, G. Martra and V. Maurino, *ACS Catal.*, 2019, **9**, 6692-6697.

(55) M. J. Uddin, F. Cesano, A. R. Chowdhury, T. Trad, S. Cravanzola, G. Martra, L. Mino, A. Zecchina and D. Scarano, *Front. Mater.*, 2020, **7**, 192.

(56) Á. Morales-García, O. Lamiel-García, R. Valero and F. Illas, *J. Phys. Chem. C*, 2018, **122**, 2413-2421.

(57) V. Blum, R. Gehrke, F. Hanke, P. Havu, V. Havu, X. Ren, K. Reuter and M. Scheffler, *Comput. Phys. Commun.*, 2009, **180**, 2175-2196.

(58) J. P. Perdew, K. Burke and M. Ernzerhof, *Phys. Rev. Lett.*, 1996, **77**, 3865-3868.

(59) C. Chang, M. Pelissier and M. Durand, *Phys. Scr.*, 1986, **34**, 394-404.

(60) L. Mino, C. Negri, R. Santalucia, G. Cerrato, G. Spoto and G. Martra, *Molecules*, 2020, **25**, 4605.

(61) A. Mandavi-Shakib, J. M. Arce-Ramos, R. N. Austin, T. J. Schwartz, L. C. Grabow and B. G. Frederick, *J. Phys. Chem. C*, 2019, **123**, 24533-24548.

(62) M. Primet, P. Pichat and M. V. Mathieu, *J. Phys. Chem.*, 1971, **75**, 1216-1220.

(63) A. A. Tsyganenko and V. N. Filimonov, *J. Mol. Struct.*, 1973, **19**, 579-589.

(64) C. Deiana, E. Fois, S. Coluccia and G. Martra, *J. Phys. Chem. C*, 2010, **114**, 21531-21538.

(65) L. Mino, F. Cesano, D. Scarano, G. Spoto and G. Martra, *Res. Chem. Intermed.*, 2019, **45**, 5801-5829

(66) C. Chizallet, M. Digne, C. Arrouvel, P. Raybaud, F. Delbecq, G. Costentin, M. Che, P. Sautet and H. Toulhoat, *Top. Catal.*, 2009, **52**, 1005-1016.

(67) C. Liu, Q. X. Ma, H. He, G. Z. He, J. Z. Ma, Y. C. Liu and Y. Wu, *Environ.-Sci. Nano*, 2017, **4**, 2388-2394.

(68) S. Dzwigaj, C. Arrouvel, M. Breysse, C. Geantet, S. Inoue, H. Toulhoat and P. Raybaud, *J. Catal.*, 2005, **236**, 245-250.

(69) C. Arrouvel, M. Digne, M. Breysse, H. Toulhoat and P. Raybaud, *J. Catal.*, 2004, **222**, 152-166.